Polyphenylene as an Active Support for Ru Catalyzed Hydrogenolysis of 5-Hydroxymethylfurfural

Qiming Wang,[†] Xuze Guan,[†] Liqun Kang,[†] Bolun Wang,[†] Lin Sheng,[†] and Feng Ryan Wang[†]*

† *Department of Chemical Engineering, University College London, Torrington Place, WC1E 7JE, London, United Kingdom;* Email: ryan.wang@ucl.ac.uk.

KEYWORDS: support-reactant/metal/solvent interaction, swelling-impregnation, 5-hydroxymethylfurfural, hydrogenolysis, catalyst reactivation

ABSTRACT: Selective transformation of biomass feedstock to platform molecules is a key pursuit for sustainable chemical production. Compared to petrochemical processes, biomass transformation requires the defunctionalization of highly polar molecules at relatively low temperatures. As a result, catalysts based on functional organic polymers may play a prominent role. Targeting the hydrogenolysis of platform chemical 5-hydroxymethylfurfural (5-HMF), here we design polyphenylene (PPhen) framework with purely sp^2-hybridized carbons that can isolate 5-HMF *via* π-π stacking, preventing hemiacetal and humins formation. With good swellability,

the PPhen framework here has successfully supported and dispersed seven types of metal particles *via* a newly developed swelling-impregnation method, including Ru, Pt, Au, Fe, Co Ni and Cu. Ru/PPhen is studied for 5-HMF hydrogenolysis, achieving 92% yield of 2,5-dimethylfuran (DMF) at mild conditions, outperforming the state-of-art catalysts reported in the literature. In addition, the PPhen helps perform a solventless reaction, achieving direct 5-HMF to DMF conversion in the absence of any liquid solvent or reagent. This approach in designing support-reactant/solvent/metal interactions will play an important role in surface catalysis.

Introduction

Biomass is a major component in renewable resources. In the future, an increased range of products will be based on biomass derived chemicals.[1-4] The processes for biomass conversion are predominantly defunctionalisation reactions, where highly oxyfunctionalized molecules are reduced in their O/C ratio.[5-7] This is completely different from petrochemical process nowadays, which are based on the reactions between hydrocarbon molecules. Reactions for biomass transformation are typically conducted in the liquid phase at moderate temperatures and proceed in a polar solvent.[8-10] These process requirements call for catalysts innovations with new molecular structure, physical geometry and surface properties. While most of the research in the field of biomass focus on the design and modification of metal catalysts, the support that helps disperse those metals also plays an important role in support-reactant, support-metal and support-solvent interactions.

Porous organic materials are viable supports for selective biomass molecule transformations. They offer controlled porosity, processability and surface variation,[11] and are used in gas storage and separation,[12, 13] drug release,[14] catalysis, sensing[15] and membrane separation.[16] Polymeric structures provide an organic surface environment and a dynamic structure upon external stimulation,[17] offering an innovative way to disperse, stabilize or activate biomass molecules at the surface.[18] As a result, they can simultaneously establish solvent-like reaction environments and post-reaction separation of the product from the solid polymers.[19, 20]

Here we report the design of a polyphenylene (PPhen)-based polymeric framework for the hydrogenolysis of platform chemical 5-Hydroxymethylfurfural (5-HMF). The PPhen simultaneously offers high porosity and swellability, due to its pure sp^2 carbon framework that retains the covalent crosslinks in the *xy*-plane, while facilitating π-π stacking in the *z* axis. This enables high loading and dispersion of metal nanoparticles *via* a newly designed swelling-impregnation method, achieving well-dispersed Ru, Pt, Au, Fe, Co, Ni and Cu particles. The Ru/PPhen achieves 92% yield of 2,5-dimethylfuran (DMF) at moderate reaction conditions (160 °C) with a low Ru/HMF molar ratio (2.8%). This result, with a low Ru/HMF molar ratio exceeds the best reported PtCo catalysts[21] and our previously reported Ru/C catalysts.[22] The phenylene and tetra-substituted benzene groups in the PPhen framework interact and isolate 5-HMF molecule, showing an 18 cm^{-1} blue shift in the aldehyde C=O stretching. This helps prevent the intermolecular hemiacetal formation, which generally leads to unwanted humins as a side product.[23] The PPhen framework serves as a functional support that participates in the

transformation of biomass molecules, rendering its potential in achieving desired reaction environments that can stabilize key intermediate states in catalysis. In addition, the PPhen interacts with both metals and 5-HMF, achieving the conversion to DMF without the presence of any liquid solvent, offering the potential for solvent-free chemical transformations.

Experimental Methods

Materials. 5-hydroxymethylfurfural (≥ 99%), 1,2,4,5-tetrabromobenzene (≥ 95.0%), tetrakis(triphenylphosphine)palladium (99%), chloroplatinic acid hexahydrate(≥ 37.5%, Pt basis), gold(III) chloride hydrate (50% Au basis), iron (III) choride (97%), cobalt(II) chloride (97%), nickel (II) chloride hexahydrate, copper (II) chloride, Ruthenium (III) Chloride (99.9%, 37% ruthenium) and benzene-1,4-diboronic acid (≥95.0%) were purchased from Sigma-Aldrich. Dichloromethane (≥99.5%), hydrochloric acid (37%), tetrahydrofuran (99.9%) and methanol (≥99.5%) were bought from Fisher Chemicals. Hydrogen peroxide (30%) and Dodecane (99%) were purchased from VWR.

Synthesis of PPhen. 1,2,4,5-tetrabromobenzene (1.531 g, 3.89 mmol) and benzene-1,4-diboronic acid (1.289 g, 7.78 mmol) were added to 120 mL of dimethylformamide. The mixture was degassed through three freeze-pump-thaw cycles. K_2CO_3 (2.0 M, 15 mL) and $Pd(PPh_3)_4$ (0.3 g, 0.25 mmol) were then added with three subsequent freeze-pump-thaw cycles. The mixture was purged with Ar and heated to 150 °C for 20 h under stirring. The product precipitated in water, and was washed by water, dichloromethane and methanol. Approximately 600 mg of grey

product was obtained in each batch. The Pd nanoparticles are removed with a mixture of hydrochloric acid and hydrogen peroxide solution at 60 ˚C.

Synthesis of PPhen loaded metal catalysts. $RuCl_3$ (Ru 38%, 58 mg, 0.22 mmol) was dissolved in ethanol (0.18 ml) and then impregnated into the PPhen powder (200 mg) under stirring until mixed uniformly, then dried at 60 ˚C. The mixture was heated at 220 ˚C under 15% hydrogen/argon for 3 h to form Ru/PPhen. For other metals, a desired amount of H_2PtCl_6, $HAuCl_4$, $FeCl_3$, $CoCl_2$, $NiCl_2$ and $CuCl_2$ were used as the precursors.

Hydrogenolysis of 5-hydroxymethylfurfural (HMF). For a typical experiment, HMF (27 mg, 0.22 mmol), tetrahydrofuran (THF, 1 ml), dodecane (1.8 mg, 0.011 mmol as internal standard) and different amounts of catalyst were added into a stainless-steel reactor and purged with hydrogen. The reaction was performed with 10 bar of initial hydrogen pressure under magnetic stirring. The reactor was cooled with ice after the reaction and the filtered solution was analyzed by gas chromatography-mass spectrometry (GC-MS). The catalysts were recycled by filtration.

Characterization. Transmission electron microscopy (TEM) was performed using a JEOL JEM−2100 microscope and ARM 200CF microscope at 200 kV. The latter is equipped with detectors for bright-field (BF), high-angle annular dark-field (HADDF) detectors. X-ray diffraction (XRD) measurements were performed using a StadiP diffractometer from STOE. X-ray photoelectron spectrum (XPS) analyses were performed on a Thermoscientific XPS K-alpha surface analysis machine using an Al source. Nitrogen adsorption–desorption isotherms were recorded at 77 K using a Micromeritics 3Flex surface characterization analyser. Microwave plasma-atomic emission spectroscopy (MP-AES) measurement was carried out with Agilent 4200 MP-AES. X-ray absorption near edge structure (XANES) and EXAFS analysis of the Ru K

edge (22.117 keV) were carried out at the P64 beamline at PetraIII DESY (Germany). Samples were diluted with boron nitride and pressed to form 1.3 cm diameter pellets for transmission measurements. Ru foil and RuO_2 were measured as standards for energy shift calibration. Demeter XAFS software package (including Athena and Artemis software) was used for XAFS data analysis. Raman spectra were recorded on a Renishaw InVia Raman spectrometer in a back-scattered confocal configuration using 647 nm laser excitation. Solid-state ^{13}C NMR spectrometer is measured with a widebore 7 T magnet, Avance 300 console, magic-angle spinning and wideline probes. FT-IR spectra were performed on Bruker Alpha FTIR spectrometer.

Results and discussion

PPhen-HMF Interaction. PPhen is synthesized through the palladium-catalyzed cross-coupling reaction of 1,2,4,5-tetrabromobenzene and benzene-1,4-diboronic acid as reported previously (Figure 1a).[24] H_2O_2-HCl mix-solution is used to remove the Pd residues in the PPhen framework, obtaining a metal free PPhen. The PPhen is mainly composed of sp^2 carbon, as shown in the solid-state ^{13}C nuclear magnetic resonance (NMR) spectroscopy, with connected sp^2 carbon and the C-H sp^2 carbon at 139.9 and 129.0 ppm, respectively (Figure 1b). Raman spectroscopy further confirms the presence of mainly aromatic groups in the PPhen, showing a typical plane stretching motion of sp^2 carbon at 1605 cm^{-1} with a small band at 1318 cm^{-1} representing the disordered sp^2 carbon (Figure 1c, red). This is essentially similar to the Raman spectra of the graphite (Figure 1c, black). The sp^2 carbon framework boosts the stability of

PPhen, remaining intact in air up to 400 ˚C. The PPhen is microporous, showing a typical type I shape of isotherm in the N_2 physisorption (Figure S1). In the presence of solvents such as ethanol, the PPhen undergoes swelling, which opens the layer to layer distance. This leads to the expansion of total polymer volume, at a linear expansion rate of $217\% \cdot ml \cdot g^{-1}$, proportional to the amount of ethanol added (Figure 1d and Figure S2). The swelling of PPhen will not only enable impregnation of metal nanoparticles but also boost the accessibility of active centres in liquid phase reactions.[25]

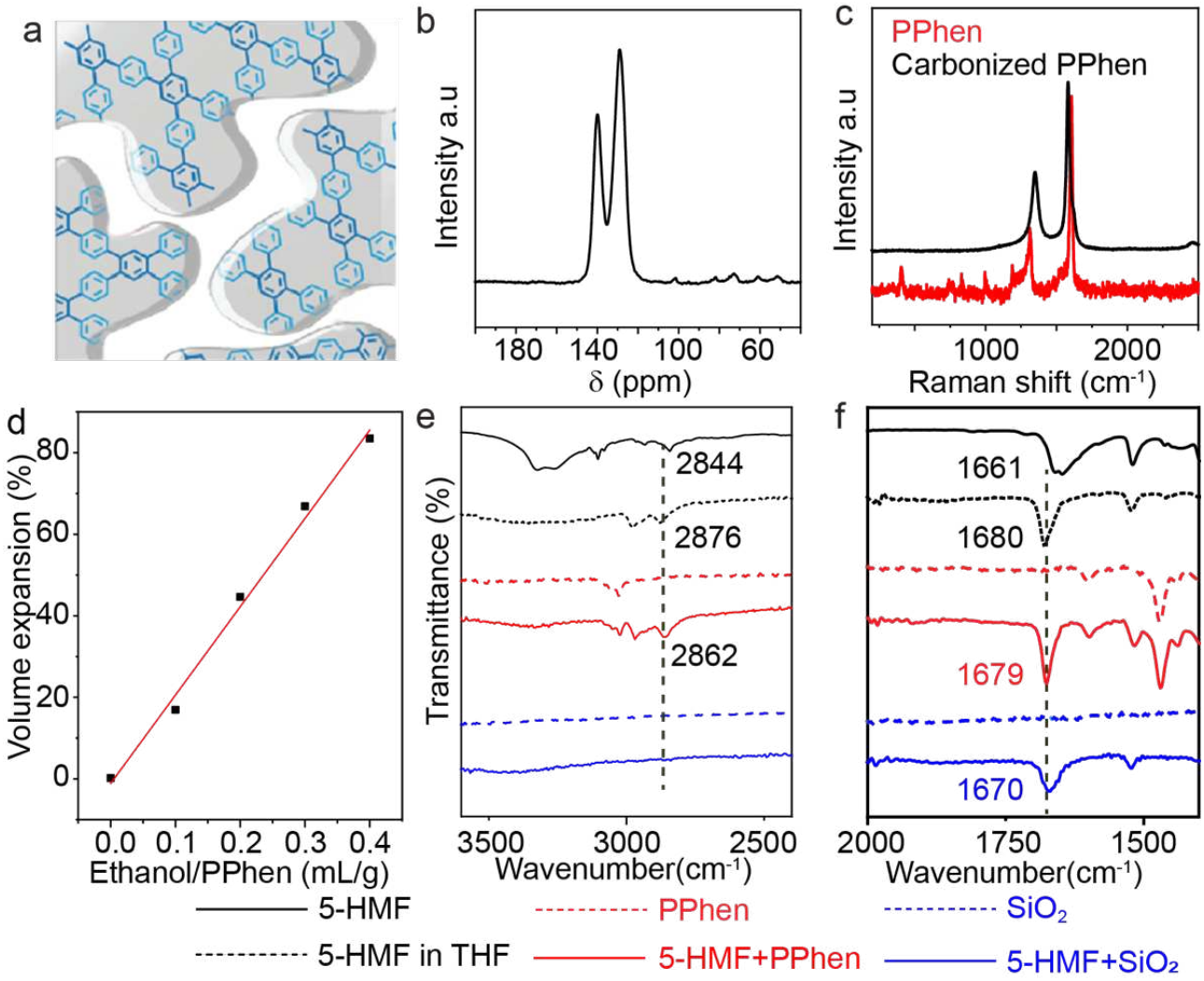

Figure 1. (a) Schematic of the PPhen structure containing phenylene and tetra-substituted benzene groups. (b) Solid state ^{13}C NMR spectra of PPhen. (c) Raman spectra of PPhen and PPhen carbonized at 900 °C. (d) Experiment (black) and fitted data (red) of PPhen volume expansion as a function of ethanol/PPhen ratio. (e,f) FTIR spectra of solid 5-HMF powder (black), physical mixture of 5-HMF over PPhen (red) and 5-HMF over SiO_2 (blue) in the regions of 2500 to 3500 cm^{-1} and 1400 to 2000 cm^{-1}, respectively. The full range spectra are shown in Figure S4.

The phenylene and tetra-substituted benzene groups within PPhen isolate and disperse 5-HMF molecules at the surface. This is studied *via* infrared (IR) spectroscopy by comparing 5-HMF over PPhen surface and pure 5-HMF. The 5-HMF solid shows the aldehyde C-H stretching at 2844 cm^{-1} and the C=O stretching at 1661 cm^{-1}, respectively (Figure 1e,f, black). The strong vibration between 3100 and 3400 cm^{-1} corresponds to the O-H stretching mode of H_2O molecule that is adsorbed within 5-HMF. In comparison, the physical mixture 5-HMF solid with PPhen powder leads to the increase of both aldehyde C-H and the C=O stretching to 2860 cm^{-1} and 1680 cm^{-1} respectively (Figure 1e,f, red). This is due to the formation of intermolecular hydrogen bonds between a hydroxymethyl group (CH_2OH) and an aldehyde group in the pure 5-HMF solid, weakening both the C=O bond and aldehyde C-H bond (Figure S3).[26] These hydrogen bonds increase the rate of hemiacetal reactions, leading to the formation of unwanted humins and reducing the selectivity to DMF. Liquid tetrahydrofuran (THF) solution helps disperse 5-HMF *via* the solvation effect (Figure 1e, black), but the surface 5-HMF can still be concentrated and

forms hydrogen bonds. This is shown in the C=O stretching at 1670 cm^{-1} observed in HMF on the surface of SiO_2 (Figure 1e, blue). In comparison, PPhen adsorbs 5-HMF *via* π-π stacking between the substituted benzene groups in PPhen and the furan group in 5-HMF. PPhen helps disperse and stabilize C=O bond, showing similar frequency at 1680 cm^{-1} to that of 5-HMF in THF solution. Thus, PPhen can ~~act as a solid solvent that~~ help prevent humin formation.

Swelling-impregnation of metal nanoparticles. The excellent swellability of PPhen enables a new impregnation strategy (Figure 2a). Concentrated metal precursor solution is added to PPhen, which simultaneously increases the layer to layer distance and transfers metal precursor inside the PPhen. During drying, the metal precursor is trapped within the PPhen framework and is further reduced to metal nanoparticles, achieving PPhen supported metals. 10wt% Ru clusters are loaded to prove this concept, resulting in the uniform dispersion of Ru clusters (Figure. 2b,c) and narrow size distribution at 1.0 ± 0.2 nm (Figure 2d). The energy dispersive spectroscopy (EDS) map shows similar Ru and carbon distributions (Figure 2e), suggesting the uniform dispersion of Ru within or on the surface of the PPhen. The absence of a Pd signal in the EDS spectrum confirmed the complete removal of Pd residue, leaving only Ru over PPhen (Figure S5). Loading of Ru clusters reduces the specific surface area from 695 to 561 $m^2 \cdot g^{-1}$ (Figure S1). The surface of the Ru clusters are in the positive oxidation states, as shown in the X-ray photoelectron spectroscopy (XPS) (Figure S6).

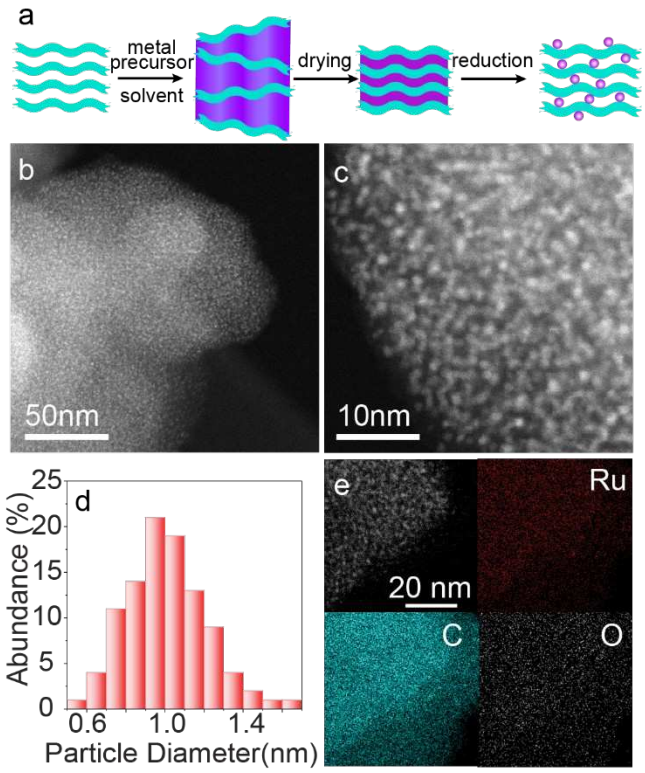

Figure 2. (a) Schematic shows the swelling-impregnation principle. (b,c) High angle annular dark field-scanning transmission electron microscopy (HADDF-STEM) images of Ru/PPhen at different length scale. (d) Corresponded size distribution histogram. (e) EDS map of Ru Lα (red), carbon Kα(green) and oxygen Kα (white).

The swelling-impregnation method is successful with supported Ru clusters. It has two advantages compared to standard wetness impregnation: 1) the ratio between the precursor solution and the support is not limited to the pore volume of the support, enabling high loadings of metal particles; 2) the removal of solvent during drying reverts the material to the original PPhen structure, providing a physical confinement effect during the crystallization of metal nanoparticles. In addition, the π-Metal interaction over the M/PPhen surface is different from the

O-M bond over the M/metal oxide surface, leading to a different metal/support interface with the metal nanoparticles.[27] We extend this method to six metal systems, including noble metals such as Pt and Au, and 3*d* metals such as Fe, Co, Ni and Cu. All six elements are widely used as heterogeneous catalysts. Within the PPhen support, noble metals form sub-nanometer clusters while 3*d* metals form nanoparticles with sizes over 10 nm (Figure 3 and Figure S7). Pt forms small clusters at 0.8 ± 0.2 nm (Figure 3a). Even at high Pt loadings such as 18wt% and 25wt%, the cluster sizes remain small at 0.9 ± 0.3 nm and 1.3 ± 0.3 nm, respectively (Figure 3b,c). The size of Au particles show bimodal distribution, with the presence of both 1.5 nm cluster and 4 nm particles (Figure 3d). In comparison, 29 ± 11 , 8 ± 3 , 10 ± 3 and 25 ± 14 nm particle sizes are measured for Fe, Co, Ni, and Cu, respectively. The Fe particles show a hexagonal shape while Co, Ni and Cu form a polyhedral shape. X-ray diffraction analysis confirms the metallic state of Pt, Co, Ru, Ni and Cu (Figure S8 and S9). CuCl is also found in the XRD pattern to show incomplete reduction. In comparison, in the case of iron, Fe_2O_3 is formed, suggesting that in these conditions the Fe^{3+} cannot be reduced by H_2. XPS analysis of Ni/PPhen, Cu/PPhen and Fe/PPhen reveals the presence of surface Ni^{2+}, Cu^{2+} and Fe^{3+}, respectively (Figure S9). The drastic difference in size distribution between noble and 3*d* metals is attributed to different rates of nucleation and growth. With the presence of H_2, the high nucleation rate of noble metals leads to small metallic clusters.

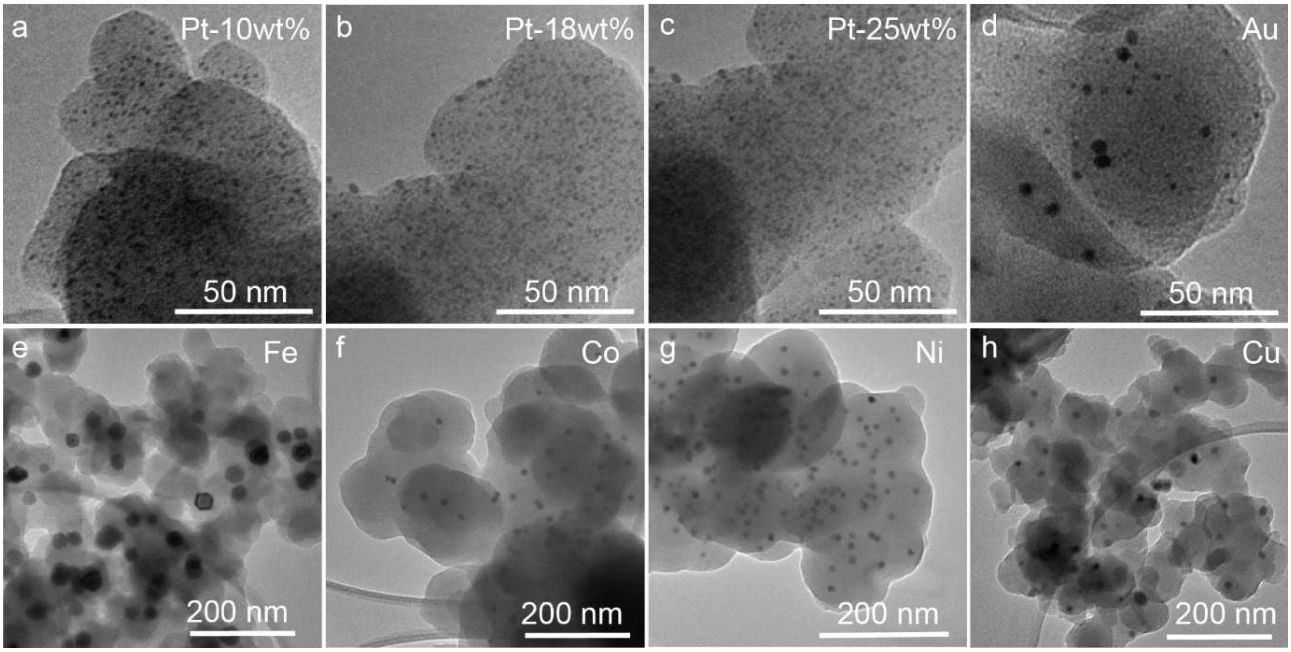

Figure 3. TEM images of (a) 10wt% Pt/PPhen, (b) 18wt% Pt/PPhen, (c) 25%wt% Pt/PPhen, (d) 2.5wt% Au/PPhen, (e) 2.5wt% Fe/PPhen, (f) 2.5wt% Co/PPhen, (g) 2.5wt% Ni/PPhen and (h) 2.5wt% Cu/PPhen.

Ru/PPhen in HMF hydrogenolysis. 2,5-DMF is a gasoline additive with a high octane number of 101.[3] The hydrogenolysis from 5-HMF to 2,5-DMF requires the cleavage of both the C-O and C=O bonds, while maintaining the furan ring. 2,5-hydroxymethylfuran (BHMF), 5-methylfurfural (5-MF) and 5-methylfuran alcohol are intermediates formed in the reaction towards 2,5-DMF. Over-hydrogenation leads to 2,5-dimethyltetrahydrofuran (DMTHF) and polymerization to humins should also be avoided. This can be achieved by controlling reaction conditions that favour the hydro-deoxygenation of C-O without hydrogenating the furan ring (Figure 4a). A survey in the literature suggests that Ru is one of the best metal catalysts for this reaction.[28, 29] THF is used as the solvent and the swelling of PPhen in THF is examined. With

only 0.1 mL/g of THF, the volume of PPhen increases by 137%, suggesting the excellent swellability and the access of reaction molecules (Figure S10). We first vary the Ru/HMF ratio in order to identify the optimized catalyst-substrate conditions. Pure PPhen shows no reactivity with 5-HMF. At 0.5% Ru/5-HMF molar ratio, 38% of HMF is converted with 11% yields of 2,5-DMF are achieved (Table S1). 5-MF is found as the intermediate product while BHMF is absent (Figure S11). This suggests that the majority of the reaction pathway follows 5-HMF→5-MF→2,5-DMF instead of 5-HMF→ BHMF →2,5-DMF (Figure 4a,b). The Ru/PPhen catalyst preferentially cleaves the C-OH bond, forming CH_3, while leaving the C=O bond untouched. Such selectivity is integral to organic chemistry and biomass conversion. Increasing the Ru/5-HMF ratio to 1.5% leads to almost full conversion of 5-HMF (93%) and the DMF yield increases to 65%. The highest yield of DMF is 92%, achieved with 2.8% Ru/5-HMF molar ratio, where the conversion of HMF remains at 93%. The result suggests that reactions catalysed with a 2.8% molar ratio can maximize the DMF formation.

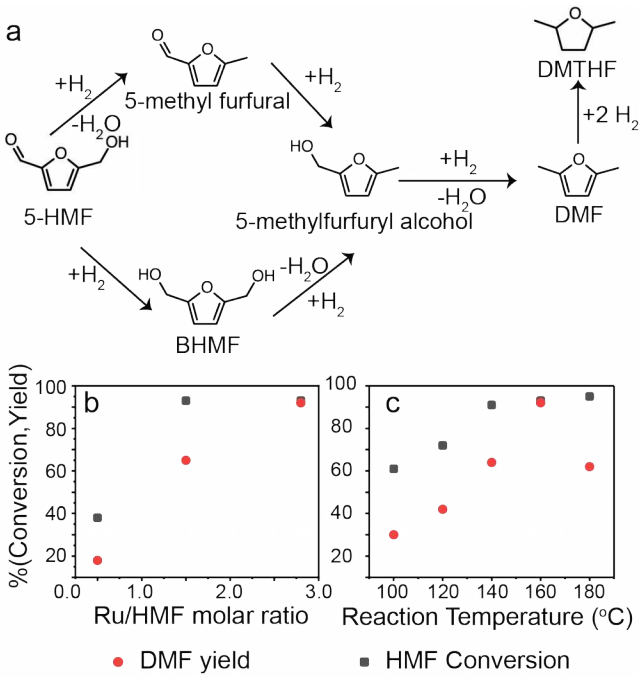

Figure 4. Hydrogenolysis of 5-HMF to 2,5-DMF. (a) Reaction pathways. (b) HMF conversion (black) and DMF yield (red), as the function of Ru/HMF molar ratio. Reaction condition: T = 160 ˚C; P = 10 bar H_2; t = 2 h. (c) HMF conversion (black) and DMF yield (red) as the function of temperature. Reaction condition: P = 10 bar H_2; t = 2 h; Ru/HMF molar ratio 2.8%.

The effect of reaction temperature is investigated while keeping the same Ru/HMF molar ratio (2.8%) and reaction time (2h). In general, both 5-HMF conversion and 2,5-DMF yield increases when the temperature is increased from 100 ˚C to 160 ˚C (Figure 4b and Table S1). It was observed that the reaction cannot be completed below 160 ˚C, as the formation of 5-methylfurfural intermediate is not fully hydrogenated to the desired product of DMF. At 180 ˚C, the yield of 2,5-DMF decreases to 62% due to over-hydrogenation, forming the undesired DMTHF side product. 93% conversion and 92% yield are achieved at 160 ˚C with 2.8 Ru/HMF

molar ratio, marking the best reaction condition for Ru/PPhen (Figure 4 and Table S1). The 99% selectivity at this condition indicates that there is no side reaction towards humin formation, which is rarely reported in the literature (Table S2).[3, 30-43] The direct comparison with Ru/commercial carbon (49% DMF yield) and Ru/SBA-15-SiO_2 (76% DMF yield) at similar conditions highlights the importance of isolating 5-HMF on the surface *via* a PPhen support.

Deactivation and reactivation of Ru/PPhen. The deactivation of the metal catalysts in hydrogenolysis is a general phenomenon, yet few reports have systematically investigated the deactivation mechanism. The recycling test has also not been performed at deferential conditions, with a conversion smaller than 20%. The dispersion of Ru clusters after catalysis was examined *via* HAADF-STEM (Figure 5a,b), to observe redistribution during catalysis. Most of the Ru clusters were observed to remain well dispersed within the PPhen framework due to the pore confinement effect, while agglomeration was seen at the edges of the PPhen particles. We hypothesize that some particles are mobile at the PPhen surface during the reaction which form agglomerates outside the pore system. This is in good agreement with our previous study, showing the agglomeration of Ru clusters outside the porous carbon channels.[22] In addition to cluster agglomeration, growth of particles is also identified, increasing from an average size of 1.0 ± 0.2 to 1.9 ± 0.6 nm (Figure 5c). Such an increase in particle size is also confirmed *via* the XRD pattern, which displays a stronger diffraction peak for metallic Ru in the cycled sample (Figure S8c). A sample of the reaction solution was withdrawn from the reactor at 160 °C and

subsequently filtered to observe the residual solution. Ru^{3+} is not detected in the MP-AES in the filtrated solution (Figure S12).

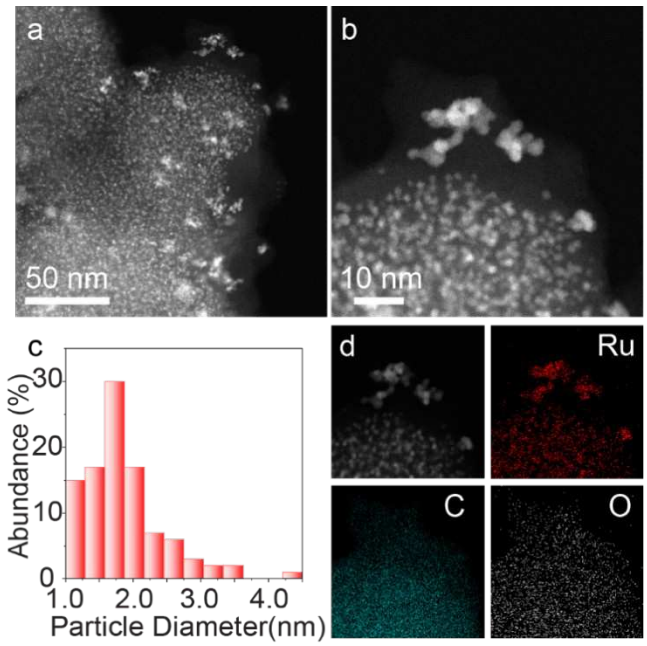

Figure 5. (a,b) HAADF-STEM images of Ru/PPhen after catalysis at different length scales. (c) The corresponding size distribution histogram. (d) EDS map of Ru Lα (red), carbon Kα (green) and oxygen Kα (white).

The increase of average particle sizes is also suggested from the X-ray absorption fine structure (XAFS) of Ru K edge. The coordination number of the first shell Ru-Ru scattering (2.73 Å) increases from 2.0 ± 0.6 to 4.1 ± 0.8, while the Ru-O scattering remains the same (Figure 6b and Table S3). This indicates an increase in the Ru particle size, resulting in more Ru atoms in the first coordination shell. Analysing the near edge, the absorption edge position shifts slightly to lower energies after catalysis, suggesting that Ru becomes more metallic (Figure 6a).

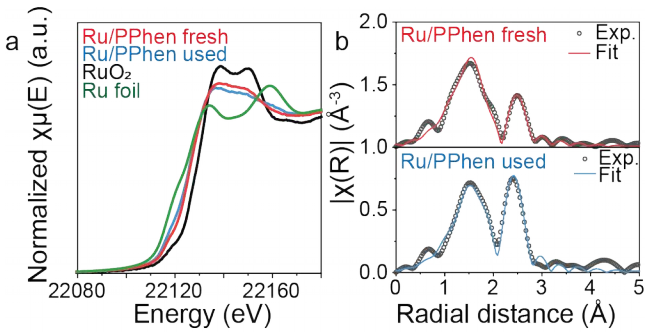

Figure 6. (a) Ru K edge X-ray absorption near edge spectroscopy (XANES) spectra of Ru foil (green), Ru/PPhen before (red), after catalysis (blue) and RuO_2 (black). (b) Experimental and fitted results of Ru/PPhen in *R*-space Extended X-ray Absorption Fine Structure (EXAFS) before (up) and after catalysis (down), respectively.

Such changes in Ru cluster size and dispersion are expected to cause a decrease in the catalytic activity. To verify this, the reaction is performed in the differential region with a low Ru/PPhen ratio of 0.5%. The initial 2,5-DMF yield is 11% while after one cycle, it drops to 4% (Figure 7a). The IR spectrum after catalysis shows additional vibrational modes between 1000 cm^{-1} to 1400 cm^{-1}, corresponding to the sp^2 C-H stretching over the furan ring (Figure 7b,c). This indicates the formation of surface furan derivatives during the reaction, which can block the active Ru surface. To reactivate the catalysts, H_2 and consecutive O_2 are used to remove the surface furan derivatives, leading to higher 2,5-DMF yields of 6 and 7% (Figure. 7a and Table S4). IR spectra after H_2 and O_2 treatment confirm the removal of the furan species and the reactivation of the Ru/PPhen catalysts. The IR spectra agree well with the carbon 1s XPS (Figure S6 and Table S5),

in which the representative C=O contribution increases after reaction and decreases to the original state after H_2 activation.

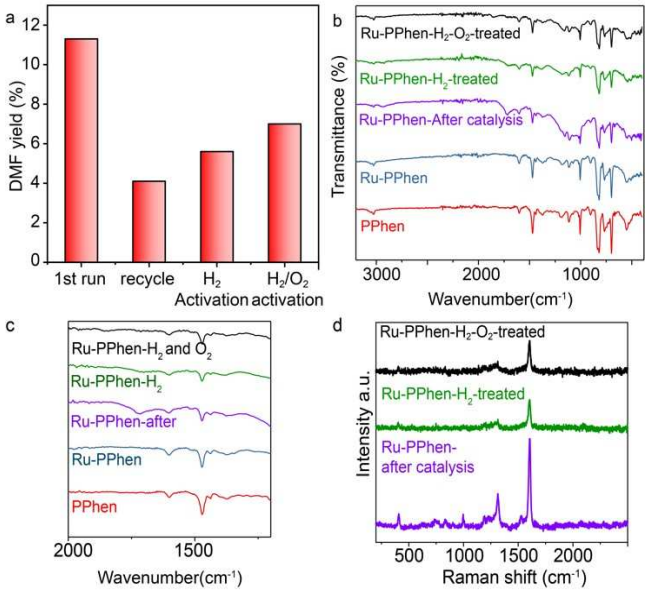

Figure 7. (a) DMF yields in the cycling performance. (b) FTIR spectra of Ru/PPhen at different activation stages. (c) Zoom-in view of FTIR spectra of Ru/PPhen at different activation stage (d) Raman spectroscopy at different stages.

The H_2 and H_2/O_2 activation mainly removes the furan species. Then PPhen framework stays intact, as confirmed by Raman spectroscopy (Figure 7d). The electronic structure of Ru is studied *via* XPS, showing no major changes in the Ru 3d peaks (Figure S6). The Ru particle size distributions are 1.4 ± 0.4 nm, and 1.7 ± 0.6 nm after H_2 and subsequent H_2 and O_2 activations, respectively (Figure S12,13). This distribution is similar to the size of Ru after catalysis (1.9 ± 0.6 nm). The aforementioned results prove that the reactivation under H_2 and O_2 is effective and does not change the structure of both Ru clusters and the PPhen support. The stability of

Ru/PPhen before and after reactions are studied with thermogravimetric analysis in air. The combustion of Ru/PPhen starts at 350 °C while that of Ru/PPhen after reaction starts at 300 °C (Figure S15). This shows that the Ru/PPhen has good stability under reaction and activation conditions.

PPhen helps stabilize 5-HMF and prevents the formation of humins, enabling the reaction in the absence of THF. It also confines most of the Ru clusters within the framework, preventing particle growth during the reaction. To prove the concept of a solventless reaction, the physical mixture of 27 mg solid 5-HMF and 6 mg Ru/PPhen is treated with 10 bar H_2 at 160 °C in the absence of any liquid. The results show the sole formation of DMF in GC-MS with no other side products (Figure S16). There is no signal for 5-HMF, indicating the complete conversion of 5-HMF to DMF. PPhen thus holds the potential of promoting liquid free catalytic reactions.

Conclusions

PPhen is designed to achieve the transformation of biomass molecules using the property of PPhen-reactant/solvent/metal interactions. PPhen mainly contains sp^2 carbon, enabling the π-π stacking between PPhen and 5-HMF. This helps isolate the 5-HMF and prevent the formation of humins. As a result, the Ru/PPhen shows 93% conversion with 99% selectivity towards 2,5-DMF at very low Ru/HMF ratios (2.8%). This result exceeds the values reported in the literature. The Ru/PPhen can also selectively cleave the C-OH bond without touching the C=O bond. Deactivation of Ru/PPhen is observed at the differential condition. The deactivated catalysts are

further activated with the presence of H_2, suggesting the needs of catalyst reactivation for this reaction. PPhen is an active organic support that can interact with reaction molecules in the absence of a liquid solvent. A swelling-impregnation method is developed for loading of noble metals and 3*d* metals onto the PPhen framework. Such a general and versatile support platform is advantageous in material innovation which improves catalysis and biomass conversions.

ASSOCIATED CONTENT

Supporting Information.

The Supporting Information is available free of charge on the ACS Publications website.

IR spectra, N_2-physisorption isotherms, XPS spectra, XRD pattern, and catalytic results are listed in Figures S1-S16 and Tables S1-S5.

AUTHOR INFORMATION

Corresponding Author

**Department of Chemical Engineering, University College London, Torrington Place, WC1E 7JE, London, United Kingdom;* Email: ryan.wang@ucl.ac.uk.

Author Contributions

The manuscript was written through contributions of all authors. All authors have given approval to the final version of the manuscript. F.R.W and Q.M.W. conceived the presented idea and wrote the manuscript. Q.M.W., X.Z.G. and B.L.W. prepared the materials and performed the catalysis. L.Q.K. contributed to the TEM and XAFS analysis. L.S. contributed to the MP-AES analysis. All authors provided critical feedback and helped shape the research, analysis and manuscript.

ACKNOWLEDGMENT

This work was conducted with the support from EPSRC projects (EP/P02467X/1, EP/S018204/1), and Royal Society research grant (RG160661), Royal Society International Exchange (IES\R3\170097, IES\R1\191035 and IEC\R3\193038). We acknowledge Diamond Light Source (SP15151, EM21370, EM19246, and MG22572). We acknowledge DESY (Hamburg, Germany), a member of the Helmholtz Association HGF, for the provision of experimental facilities. Parts of this research were carried out at Petra III and we would like to thank Dr. Wolfgang Caliebe and Dr. Vadim Murzin for assistance in using P64 beamline (I-20190358 EC). Q.M.W would like to thank the China Scholarship Council (CSC) for the PhD funding.

REFERENCES

1. Chheda, J. N.; Huber, G. W.; Dumesic, J. A. Liquid-Phase Catalytic Processing of Biomass-Derived Oxygenated Hydrocarbons to Fuels and Chemicals. *Angew. Chem. Int. Ed.* **2007,** *46*, 7164-7183.

2. Climent, M. J.; Corma, A.; Iborra, S. Conversion of Biomass Platform Molecules into Fuel Additives and Liquid Hydrocarbon Fuels. *Green. Chem.* **2014,** *16*, 516-547.

3. Roman-Leshkov, Y.; Barrett, C. J.; Liu, Z. Y.; Dumesic, J. A. Production of Dimethylfuran for Liquid Fuels from Biomass-Derived Carbohydrates. *Nature* **2007,** *447*, 982-U5.
4. Ragauskas, A. J.; Williams, C. K.; Davison, B. H.; Britovsek, G.; Cairney, J.; Eckert, C. A.; Frederick, W. J.; Hallett, J. P.; Leak, D. J.; Liotta, C. L.; Mielenz, J. R.; Murphy, R.; Templer, R.; Tschaplinski, T. The Path Forward for Biofuels and Biomaterials. *Science* **2006,** *311*, 484-489.
5. Gallezot, P. Conversion of Biomass to Selected Chemical Products. *Chem. Soc. Rev.* **2012,** *41*, 1538-1558.
6. Xu, W. Y.; Miller, S. J.; Agrawal, P. K.; Jones, C. W. Depolymerization and Hydrodeoxygenation of Switchgrass Lignin with Formic Acid. *Chemsuschem* **2012,** *5*, 667-675.
7. Huang, X. M.; Koranyi, T. I.; Boot, M. D.; Hensen, E. J. M. Catalytic Depolymerization of Lignin in Supercritical Ethanol. *Chemsuschem* **2014,** *7*, 2276-2288.
8. Rinaldi, R.; Schuth, F. Design of Solid Catalysts for the Conversion of Biomass. *Energ. Environ. Sci.* **2009,** *2*, 610-626.
9. Mellmer, M. A.; Sener, C.; Gallo, J. M. R.; Luterbacher, J. S.; Alonso, D. M.; Dumesic, J. A. Solvent Effects in Acid-Catalyzed Biomass Conversion Reactions. *Angew. Chem. Int. Ed.* **2014,** *53*, 11872-11875.
10. Taylor, M. J.; Durndell, L. J.; Isaacs, M. A.; Parlett, C. M. A.; Wilson, K.; Lee, A. F.; Kyriakou, G. Highly Selective Hydrogenation of Furfural over Supported Pt Nanoparticles under Mild Conditions. *Appl. Catal. B: Environ.* **2016,** *180*, 580-585.
11. Wu, D.; Xu, F.; Sun, B.; Fu, R.; He, H.; Matyjaszewski, K. Design and Preparation of Porous Polymers. *Chem. Rev.* **2012,** *112*, 3959-4015.
12. Wood, C. D.; Tan, B.; Trewin, A.; Su, F.; Rosseinsky, M. J.; Bradshaw, D.; Sun, Y.; Zhou, L.; Cooper, A. I. Microporous Organic Polymers for Methane Storage. *Adv. Mater.* **2008,** *20*, 1916-1921.
13. Du, N.; Robertson, G. P.; Song, J.; Pinnau, I.; Thomas, S.; Guiver, M. D. Polymers of Intrinsic Microporosity Containing Trifluoromethyl and Phenylsulfone Groups as Materials for Membrane Gas Separation. *Macromolecules* **2008,** *41*, 9656-9662.
14. Abidian, M. R.; Kim, D. H.; Martin, D. C. Conducting-Polymer Nanotubes for Controlled Drug Release. *Adv. Mater.* **2006,** *18*, 405-409.
15. Zhao, C.; Danish, E.; Cameron, N. R.; Kataky, R. Emulsion-Templated Porous Materials (Polyhipes) for Selective Ion and Molecular Recognition and Transport: Applications in Electrochemical Sensing. *J. Mater. Chem.* **2007,** *17*, 2446-2453.
16. Schacher, F.; Ulbricht, M.; Müller, A. H. Self-Supporting, Double Stimuli-Responsive Porous Membranes from Polystyrene-Block-Poly (N, N-Dimethylaminoethyl Methacrylate) Diblock Copolymers. *Adv. Funct. Mater.* **2009,** *19*, 1040-1045.

17. Liu, F.; Wang, L.; Sun, Q.; Zhu, L.; Meng, X.; Xiao, F.-S. Transesterification Catalyzed by Ionic Liquids on Superhydrophobic Mesoporous Polymers: Heterogeneous Catalysts That Are Faster Than Homogeneous Catalysts. *J. Am. Chem. Soc.* **2012,** *134*, 16948-16950.
18. Lin, Y. C.; Huber, G. W. The Critical Role of Heterogeneous Catalysis in Lignocellulosic Biomass Conversion. *Energ. Environ. Sci.* **2009,** *2*, 68-80.
19. Liu, F. J.; Kong, W. P.; Qi, C. Z.; Zhu, L. F.; Xiao, F. S. Design and Synthesis of Mesoporous Polymer-Based Solid Acid Catalysts with Excellent Hydrophobicity and Extraordinary Catalytic Activity. *ACS Catal.* **2012,** *2*, 565-572.
20. Dong, K.; Sun, Q.; Meng, X. J.; Xiao, F. S. Strategies for the Design of Porous Polymers as Efficient Heterogeneous Catalysts: From Co-Polymerization to Self-Polymerization. *Catal. Sci. Technol.* **2017,** *7*, 1028-1039.
21. Wang, G.-H.; Hilgert, J.; Richter, F. H.; Wang, F.; Bongard, H.-J.; Spliethoff, B.; Weidenthaler, C.; Schueth, F. Platinum-Cobalt Bimetallic Nanoparticles in Hollow Carbon Nanospheres for Hydrogenolysis of 5-Hydroxymethylfurfural. *Nat. Mater.* **2014,** *13*, 294-301.
22. Xu, R.; Kang, L.; Knossalla, J.; Mielby, J.; Wang, Q.; Wang, B.; Feng, J.; He, G.; Qin, Y.; Xie, J.; Swertz, A.-C.; He, Q.; Kegnas, S.; Brett, D. J. L.; Schuth, F.; Wang, F. R. Nanoporous Carbon: Liquid-Free Synthesis and Geometry-Dependent Catalytic Performance. *ACS Nano* **2019** *13*, 2463-2472.
23. Tsilomelekis, G.; Josephson, T. R.; Nikolakis, V.; Caratzoulas, S. Origin of 5-Hydroxymethylfurfural Stability in Water/Dimethyl Sulfoxide Mixtures. *Chemsuschem* **2014,** *7*, 117-126.
24. Wang, F.; Mielby, J.; Richter, F. H.; Wang, G.; Prieto, G.; Kasama, T.; Weidenthaler, C.; Bongard, H.-J.; Kegnaes, S.; Fuerstner, A.; Schueth, F. A Polyphenylene Support for Pd Catalysts with Exceptional Catalytic Activity. *Angew. Chem. Int. Ed.* **2014,** *53*, 8645-8648.
25. Sidorov, S. N.; Volkov, I. V.; Davankov, V. A.; Tsyurupa, M. P.; Valetsky, P. M.; Bronstein, L. M.; Karlinsey, R.; Zwanziger, J. W.; Matveeva, V. G.; Sulman, E. M.; Lakina, N. V.; Wilder, E. A.; Spontak, R. J. Platinum-Containing Hyper-Cross-Linked Polystyrene as a Modifier-Free Selective Catalyst for L-Sorbose Oxidation. *J. Am. Chem. Soc.* **2001,** *123*, 10502-10510.
26. Nie, B. N.; Stutzman, J.; Xie, A. H. A Vibrational Spectral Maker for Probing the Hydrogen-Bonding Status of Protonated Asp and Glu Residues. *Biophys. J.* **2005,** *88*, 2833-2847.
27. Cargnello, M.; Grzelczak, M.; Rodriguez-Gonzalez, B.; Syrgiannis, Z.; Bakhmutsky, K.; La Parola, V.; Liz-Marzan, L. M.; Gorte, R. J.; Prato, M.; Fornasiero, P. Multiwalled Carbon Nanotubes Drive the Activity of Metal@Oxide Core-Shell Catalysts in Modular Nanocomposites. *J. Am. Chem. Soc.* **2012,** *134*, 11760-11766.
28. Chen, S.; Wojcieszak, R.; Dumeignil, F.; Marceau, E.; Royer, S. How Catalysts and Experimental Conditions Determine the Selective Hydroconversion of Furfural and 5-Hydroxymethylfurfural. *Chem. Rev.* **2018,** *118*, 11023-11117.

29. Wang, H. Y.; Zhu, C. H.; Li, D.; Liu, Q. Y.; Tan, J.; Wang, C. G.; Cai, C. L.; Ma, L. L. Recent Advances in Catalytic Conversion of Biomass to 5-Hydroxymethylfurfural and 2, 5-Dimethylfuran. *Renew. Sust. Energ. Rev.* **2019,** *103*, 227-247.
30. Zhu, Y.; Kong, X.; Zheng, H.; Ding, G.; Zhu, Y.; Li, Y.-W. J. C. S.; Technology. Efficient Synthesis of 2, 5-Dihydroxymethylfuran and 2, 5-Dimethylfuran from 5-Hydroxymethylfurfural Using Mineral-Derived Cu Catalysts as Versatile Catalysts. *Catal. Sci. Technol.* **2015,** *5*, 4208-4217.
31. Hu, L.; Tang, X.; Xu, J.; Wu, Z.; Lin, L.; Liu, S. J. I. Selective Transformation of 5-Hydroxymethylfurfural into the Liquid Fuel 2, 5-Dimethylfuran over Carbon-Supported Ruthenium. *Ind. Engineer. Chem. Res.* **2014,** *53*, 3056-3064.
32. Zu, Y.; Yang, P.; Wang, J.; Liu, X.; Ren, J.; Lu, G.; Wang, Y. J. A. C. B. E. Efficient Production of the Liquid Fuel 2, 5-Dimethylfuran from 5-Hydroxymethylfurfural over Ru/Co_3O_4 Catalyst. *Appl. Catal. B-Envir.* **2014,** *146*, 244-248.
33. Nagpure, A. S.; Lucas, N.; Chilukuri, S. V. Efficient Preparation of Liquid Fuel 2, 5-Dimethylfuran from Biomass-Derived 5-Hydroxymethylfurfural over Ru–Nay Catalyst. *ACS Sustain. Chem. Eng.* **2015,** *3*, 2909-2916.
34. Yang, Y.; Liu, Q.; Li, D.; Tan, J.; Zhang, Q.; Wang, C.; Ma, L. Selective Hydrodeoxygenation of 5-Hydroxymethylfurfural to 2, 5-Dimethylfuran on Ru–MoO X/C Catalysts. *RSC Adv.* **2017,** *7*, 16311-16318.
35. Kong, X.; Zhu, Y.; Zheng, H.; Dong, F.; Zhu, Y.; Li, Y.-W. Switchable Synthesis of 2, 5-Dimethylfuran and 2, 5-Dihydroxymethyltetrahydrofuran from 5-Hydroxymethylfurfural over Raney Ni Catalyst. *RSC Adv.* **2014,** *4*, 60467-60472.
36. Yang, P.; Cui, Q.; Zu, Y.; Liu, X.; Lu, G.; Wang, Y. Catalytic Production of 2, 5-Dimethylfuran from 5-Hydroxymethylfurfural over Ni/Co_3O_4 Catalyst. *Catal. Commun.* **2015,** *66*, 55-59.
37. Chen, B.; Li, F.; Huang, Z.; Yuan, G. Carbon-Coated Cu-Co Bimetallic Nanoparticles as Selective and Recyclable Catalysts for Production of Biofuel 2, 5-Dimethylfuran. *Appl. Catal. B: Environ.* **2017,** *200*, 192-199.
38. Yang, P.; Xia, Q.; Liu, X.; Wang, Y. Catalytic Transfer Hydrogenation/Hydrogenolysis of 5-Hydroxymethylfurfural to 2, 5-Dimethylfuran over Ni-Co/C Catalyst. *Fuel* **2017,** *187*, 159-166.
39. Seemala, B.; Cai, C. M.; Wyman, C. E.; Christopher, P. Support Induced Control of Surface Composition in Cu–Ni/Tio2 Catalysts Enables High Yield Co-Conversion of Hmf and Furfural to Methylated Furans. *ACS Catal.* **2017,** *7*, 4070-4082.
40. Velez, R. P.; Ellmers, I.; Huang, H.; Bentrup, U.; Schuenemann, V.; Gruenert, W.; Brueckner, A. Identifying Active Sites for Fast NH3-SCR of NO/NO_2 Mixtures over Fe-ZSM-5 by Operando EPR and UV-Vis Spectroscopy. *J. Catal.* **2014,** *316*, 103-111.
41. Yu, L.; He, L.; Chen, J.; Zheng, J.; Ye, L.; Lin, H.; Yuan, Y. Robust and Recyclable Nonprecious Bimetallic Nanoparticles on Carbon Nanotubes for the Hydrogenation and Hydrogenolysis of 5-Hydroxymethylfurfural. *ChemCatChem* **2015,** *7*, 1701-1707.

42. Kong, X.; Zheng, R.; Zhu, Y.; Ding, G.; Zhu, Y.; Li, Y.-W. Rational Design of Ni-Based Catalysts Derived from Hydrotalcite for Selective Hydrogenation of 5-Hydroxymethylfurfural. *Green. Chem.* **2015,** *17*, 2504-2514.
43. Li, J.; Zhang, J. j.; Liu, H. y.; Liu, J. l.; Xu, G. y.; Liu, J. x.; Sun, H.; Fu, Y. Graphitic Carbon Nitride (G-C_3N_4)-Derived Fe-N-C Catalysts for Selective Hydrodeoxygenation of 5-Hydroxymethylfurfural to 2, 5-Dimethylfuran. *ChemistrySelect* **2017,** *2*, 11062-11070.

BRIEFS

For Table of Contents Only

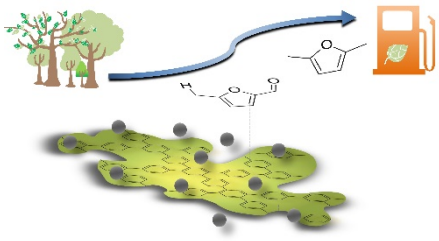

Polyphenylene is a versatile platform to confine active catalytic component and disperse reaction molecules, enabling biofuel production from 5-Hydroxymethylfurfural.